Tunable Fano quantum-interference dynamics using a topological phase transition in $(Bi_{1-x}In_{x})_{2}Se_{3}$

Sangwan Sim, Nikesh Koirala, Matthew Brahlek, Ji Ho Sung, Jun Park, Soonyoung Cha, Moon-Ho Jo, Seongshik Oh, and Hyunyong Choi

Phys. Rev. B **91**, 235438 — Published 23 June 2015

DOI: 10.1103/PhysRevB.91.235438

Tunable Fano quantum-interference dynamics using topological phase transition in $(Bi_{1-x}In_x)_2Se_3$

Sangwan Sim,[1] Nikesh Koirala,[2] Matthew Brahlek,[2] Ji Ho Sung,[3,4] Jun Park,[1] Soonyoung Cha,[1] Moon-Ho Jo,[3,4,5] Seongshik Oh,[2,6] and Hyunyong Choi[1,*]

[1]*School of Electrical and Electronic Engineering, Yonsei University, Seoul 120-749, Korea*

[2]*Department of Physics and Astronomy, Rutgers the State University of New Jersey, Piscataway, New Jersey 08854, USA*

[3]*Center for Artificial Low Dimensional Electronic Systems, Institute for Basic Science (IBS), Pohang University of Science and Technology (POSTECH), 77 Cheongam-Ro, Pohang 790-784, Korea*

[4]*Division of Advanced Materials Science, Pohang University of Science and Technology (POSTECH), 77 Cheongam-Ro, Pohang 790-784, Korea*

[5]*Department of Materials Science and Engineering, Pohang University of Science and Technology (POSTECH), 77 Cheongam-Ro, Pohang 790-784, Korea*

[6]*Institute for Advanced Materials, Devices and Nanotechnology, Rutgers the State University of New Jersey, Piscataway, New Jersey 08854, USA*

PACS numbers: 78.47.da, 78.47.db, 73.20.-r, 73.50.Gr

Abstract

Asymmetric Fano resonance arise from quantum interference between discrete and continuum state. The characteristic asymmetry has attracted strong interests in understanding light-induced optoelectronic responses and corresponding applications. In conventional solids, however, the tunability of Fano resonance is generally limited by material's intrinsic

[*]E-mail: hychoi@yonsei.ac.kr

property. Topological insulators are unique states of matters embodying both conducting Dirac surface and underlying bulk. If it is possible to manipulate the two coexisting states, then it should form an ideal laboratory for realizing a tunable topological Fano system. Here, with recently discovered topological phase transition in $(Bi_{1-x}In_x)_2Se_3$, we report new tunable Fano interference phenomena. By engineering the spatial overlap between surface Dirac electrons (continuous terahertz transitions) and bulk phonon (discrete mode at ~ 2 terahertz), we continuously tune, abruptly switch, and dynamically modulate the Fano resonance. Eliminating the topological surface via decreasing spin-orbit coupling—that is, across topological and non-topological phase, we find that the asymmetric Fano spectra return to the symmetric profile. Laser-excited ultrafast terahertz spectroscopy reveals that the controlled spatial overlap is responsible for the picosecond tunability of the Fano resonance, suggesting potentials toward optically controllable topological Fano systems.

I. INTRODUCTION

Topological insulators (TIs) are novel classes of quantum systems, where the gapped bulk state with strong spin-orbit coupling (SOC) hosts the gapless Dirac surface states [1–4]. The formation of topological surface state (TSS) results from the strong SOC-induced bulk band inversion [1]. Recent investigations have shown that it is possible to demonstrate continuous gap opening and TSS elimination with vanishing bulk band inversion in $TlBi(S_{1-x}Se_x)_2$ and $(Bi_{1-x}In_x)_2Se_3$ [5–9]. These processes, via modulating the SOC or lattice constant, lead to so called "quantum phase transition" from the topological phase (that is with the TSS) to the non-topological phase (that is without TSS). Such capability provides an exciting opportunity to explore the surface-surface hybridization and Dirac-dispersion engineering.

One seminal feature of TIs is that the conducting Dirac surface and the underlying bulk coexist. For this reason, when light excitation takes place, TIs could be ideal platforms for manipulating the coupling between the two states. The most prominent example to investigating this coupling is the Fano interference. The quantum-mechanical transition mixing between the continuous and the discrete states leads to the characteristic Fano resonance, whose degree of asymmetry is directly related to the interference strength [10–14]. More importantly, controlling the Fano resonance or tuning such quantum interference may offer novel ways to design optoelectronically tunable Fano systems. In TIs, the coexistence nature of surface and bulk state is expected to serve as a unique testbed for examining the topologically tunable Fano resonance.

Here, we show that the Fano resonance can be manipulated by controlling the topological phase transition in $(Bi_{1-x}In_x)_2Se_3$. In the process of the topological phase transition, it influences the low-energy Dirac surface such that underlying bulk electronic property is

strongly correlated with the surface electrons. Depending on the SOC-induced bulk band inversion, it is possible to engineer the spatial overlap between the surface and the bulk; in the $(Bi_{1-x}In_x)_2Se_3$ system, this can be achieved by replacing a heavy Bi atom with a lighter In atom, thereby controlling the SOC [8,9]. In our study, we experimentally demonstrate that the spatial overlap between the surface Dirac wavefunctions and the discrete bulk phonon indeed play a key role in determining the tunability of Fano resonance. Stepping further, we experimentally demonstrated that this Fano resonance can be optically modulated on a piscosecond (ps) time scale under femtosecond optical excitation.

Figure 1 is the conceptual schematic illustrating the tunable Fano resonance using topological quantum phase transition. In the $(Bi_{1-x}In_x)_2Se_3$ system, the electronic transitions both for the gapless metallic Dirac electrons and the discrete bulk phonon are located in the terahertz (THz) frequency range; the former is graphene-like continuous THz transitions and the latter is discrete bulk phonon located at ~ 2 THz [9,15,16]. Figure 1(a) show the case of conventional TI. In absence of In atoms, the spatial division between the Dirac electronic transitions and the phonon mode is far substantial, therefore the interference strength is relatively small, which results in small Fano asymmetry. Figure 1(b) is the case of large Fano asymmetry. With increasing In-concentration, the TSS wavefunction penetrates more deeply into the bulk. The Fano spectra are strongly re-shaped and the conductance profile undergoes a strongly asymmetric shape due to the enhanced spatial overlap between the surface and the bulk. Figure 1(c) illustrates the effect of optical excitation at this situation. When laser excitation occurs, hot-carriers relaxation takes place from the bulk to the surface. In this regime, because of the strong TSS-bulk spatial overlap, it is possible to dynamically change the Fano resonance on a ps time scale.

II. TOPOLOGICALLY TUNABLE FANO INTERFERENCE

In order to understand the relationship between the topological phase transition and the Fano resonance, it is instructive to review the effect of In-atom substitution on the topological phase transition [8,9]. Three main aspects are addressed here. First, one of necessary conditions for the TSS formation is the strong SOC-induced band inversion between the valence band minimum and the conduction band maximum. Figure 2(a) illustrates this band inversion in the topological phase with upper gray and lower black parabolas, where the Dirac-like TSSs exist on the surfaces with large spatial separation from the bulk. As In-substitution increases, SOC becomes weaker, and the band inversion is gradually relaxed. The decreased SOC eventually turns off the band inversion, resulting in closing and re-opening the bulk band gap—a transition point is called "topological quantum critical point". At this transition point, the topological phase transition occurs, and the bulk-gap is completely closed. In our case, this is when the In-concentration is approximately ~ 6 % [9]. Second, when the In-concentration is above the critical point, the bulk band gap re-opens without band inversion. The system enters into the non-topological phase without TSSs. This is illustrated by upper black and lower gray parabolas (see the non-topological phase in Figure 2(a). Third, it is important to note that the In-atom substitution also changes the spatial overlap of wavefunctions between the TSS and the bulk. It has been predicted and later experimentally observed that the penetration depth δ of the TSS wavefunctions into the bulk is inversely proportional to the bulk gap size [8,9,17]. Thus, as the topological phase approaches the topological quantum critical point, it should be possible to manipulate the spatial overlap between TSS and the bulk. This is schematically shown as yellow regions (TSS wavefunctions) and gray squares (bulk) in the upper row of Figure 2(a).

To investigate the effect of topological phase transition on the Fano spectra, we first performed the THz time-domain spectroscopy in equilibrium (without optical excitation) [18]. The samples are MBE-grown high quality $(Bi_{1-x}In_x)_2Se_3$ thin films containing 50 quintuple layers (QLs) with different In-concentration ranging from 0 % to 10 % (see Appendix A for the sample growth). Figure 2(b) is the measured THz conductance spectra (see Ref. [19] for the experimental setup). The observed THz sheet conductance spectra consist of Drude background, which arises from the intraband electronic transitions, and the optical phonon peak at ~ 2 THz. Prior THz measurements have shown that the former Drude signal does not vary significantly regardless of the thickness of TIs (16-100 QL), whereas the spectral weight of the latter phonon peak is strongly suppressed as the thickness of TIs is reduced [9,20,21]. Thus, we attribute the Drude response and the phonon resonance to the TSS electronic transitions and the bulk lattice vibrations, respectively [9,15,20,21]. As expected from the SOC-dependent overlap between the Dirac wavefunctions and the bulk (Fig. 1 and Fig. 2(a)), the THz response varies depending on the substituted concentration of In-atom. In particular, the THz spectra are largely asymmetric as the system approaches the topological quantum critical point, and they are rapidly changed to the symmetric shapes across the topological phase transition. For more quantitative analysis, we fit them accordingly with a Drude-Fano model (see Appendix B).

For the Drude response, with increasing In-concentration, we observe that the Drude scattering rate Γ_{Drude} (Fig. 2(c)) is increased due to the substitutional disorder of In-atoms [9] (Drude spectral weight is separately discussed in Ref. [19]). Within the topological phase (In < 6 %), the width of Re(G) becomes gradually broader due to the increased Γ_{Drude}. After the topological phase transition (In ≥ 6 %), the Drude shape is abruptly flat. This is because of the sharply enhanced Γ_{Drude}, as seen in Fig. 2(c). The microscopic origin of these Drude

scattering dynamics can be understood as following. Before the topological quantum critical point, the surface Dirac electrons are topologically protected against backscattering—that is one distinct characteristic of TIs. As the quantum phase enters into the non-topological phase, this is no longer valid because the decreased SOC eliminates the TSSs. In this phase, the absence of TSSs allows the backscattering events, thereby Γ_{Drude} increases substantially. This is the origin of abrupt changes of the Drude response. Of course, some residual carriers in bulk or from the surface accumulation layer may exist even in the non-topological phase, which possibly contributes to the Drude-like response above In $\geq$ 6 % [9].

Having understood that the smoothly varying continuum originates from the Drude response, we next consider the degree of asymmetry of the Fano resonance [9,15,20]. The Fano parameter $1/q$ is widely used to quantify the measure of asymmetry (see Appendix B), which is associated with the ~ 2 THz narrow phonon peak in the TIs [9,15,20,22]. Considering the Drude response of TSS electrons, $1/q$ is a measure of interaction strength between TSS electron and bulk optical phonon. This assignment is supported by the positive $1/q$ of the observed Fano asymmetry [23–25] as displayed in Fig. 2(d) and 2(f) (see Ref. [19] for more detailed discussion about the sign of $1/q$). There, we see that $1/q$ gradually becomes larger with increasing In-concentration and shows a sudden drop as the TSS disappears. This is a direct signature representing that the Fano resonance can be controlled by presence/absence of the TSSs. The effect of TSSs on $1/q$ can be elucidated in the following way. For the 50 QLs sample, Wu *et al*. shows that δ is approximately 3 QL, 5 QL and 10 QL for In = 0 %, 2 % and 4 %, respectively [9]. Considering the sample thickness of 50 QL, the top and bottom occupy only about a tenth of the sample volume for In = 0 %. In the topological phase, the Fano asymmetry is relatively small with $1/q \sim 0.07$. On the other hand, as the system approaches the topological phase transition, i.e. In = 4 %, the asymmetry is

distinctly increased with $1/q \sim 0.25$, where the TSS overlap reaches 40 % of the bulk. Thus, we understand that the Fano asymmetry is strongest exactly when the TSS-bulk overlap is the largest. Such results are important not only because they shed light on the topological origin of the Fano resonance, but also suggest that the Fano resonance can be tunable using topological phase transition by way of spatial manipulation of the surface-bulk overlap.

Although the above examinations based on the equilibrium THz responses well account for the SOC-dependent Fano resonance, a question may evoke whether the Fano resonance purely arise from the electron dynamics of TSSs, because of the following two reasons. First, the symmetric/symmetric feature of Re(G) spectra is somewhat masked by the broadened Drude width as the In-concentration increases (Fig. 2(e)) [9]. This suggests that additional experimental evidence which can separately resolve the Drude and its coupling with the optical phonon is highly necessary. Second, we cannot exclude the non-topological factors affecting the Fano resonance, because both residual bulk electrons and the massive two dimensional electron gas (2DEG) in the surface [26] can also contribute to the Drude response [27]; as shown in Fig. 2(d), the Fano asymmetry does not completely disappear even when the TSS states are disappeared (In = 6, 10 %), representing the topologically trivial electrons partially contribute to the coupling with the bulk optical phonon.

III. ULTRAFAST FANO QUANTUM-INTERFERENCE DYNAMICS

To resolve these issues, we explore the time-resolved Fano resonance by using ultrafast optical-pump THz-probe spectroscopy, and directly compare the results with/without optical excitation [28] (see Ref. [19] for the experiment setup). Figure 3(a) shows the time-dependent conductance evolution (black circles) after 50-fs photoexcitation with 1.55 eV pump-photon energy, together with the equilibrium conductance (gray line) and Drude-Fano fit (black line).

The data were taken from a TI exhibiting a large bulk-TSS spatial overlap, i.e. In=4 %. Figure 3(b) summarizes the transient dynamics of Drude-spectral weight D_{Drude} (top panel, a measure of electron density, see Appendix B), $1/q$ (middle panel), and the phonon linewidth Γ_{ph} (bottom panel); these parameters are obtained by the Drude-Fano fit. After the pump, D_{Drude} is largely increased due to the photodoping effect, followed by relaxation toward equilibrium via electronic cooling and recombination [16,21,29–34]. The Fano parameter $1/q$ also increases with photoexcitation, however, its dynamics is distinctly different from that of D_{Drude}. As shown in Figure 3b, the rising transient of $1/q$ significantly lags behind that of D_{Drude}. In particular, although the magnitude of D_{Drude} at Δt = 0.5 and 2.5 ps is similar, $1/q$ shows much larger Fano asymmetry at Δt = 2.5 ps compared to $1/q$ at Δt = 0.5. This result is rather surprising because the Fano asymmetry (induced by phonon lineshape) generally shows an instantaneous response after photoexcitation, and the associated transient decay should closely follow the photocarrier dynamics in conventional solids, as long as the origin of asymmetry stems from the electronic coupling [35–38].

To scrutinize the details of time-dependent transients of D_{Drude} and $1/q$ dynamics, we consider below some possible electronic relaxation channels and exclude the associated contributions. After the pump excitation, the photoexcited electrons relax initially to the states near the Fermi level in the bulk conduction band, as indicated by black arrow in Fig. 3(c). Our previous study showed that the ps rising of D_{Drude} dynamics in the nominal Bi_2Se_3 TIs originates mainly from the electronic relaxation in the bulk [21]. Thus, $1/q$ dynamics should directly follow D_{Drude} dynamics, if the topologically-trivial bulk electrons are the main factor for the observed transient Fano resonance. Because we observed that the rising dynamics of $1/q$ is temporally delayed, we understand that the electronic relaxation within the

bulk electrons is not responsible for the observed Fano dynamics. For the dynamics of massive 2DEG, recent angle-resolved photoemission spectroscopy (ARPES) measurement of Bi_2Se_3 have shown that the 2DEG exhibits a sharp spectral rim around the bottom of the bulk conduction band [26]. Because the electronic band of 2DEG and bulk are closely overlapped in the E-*k* space, the rising dynamics of the two are expected to be extremely fast, exhibiting very similar transients. In addition, recently performed time-resolved ARPES study on ZnO [39] have reported that the time scale of the photoexcited carrier relaxation from the bulk conduction band to the surface 2DEG (formed by the downward band bending) is about 200 fs. This time-scale is very short compared to the observed ps rising time of D_{Drude} in our TI case. Thus, the contribution of surface 2DEG is likely small to the transient Fano resonance. We can also rule out the effect of photoinduced lattice heating or hot-phonon effect on the 1/*q* dynamics. The bottom panel in Fig. 3b shows the phonon linewidth (Γ_{ph}) dynamics, exhibiting a very slowly increasing feature compared to the 1/*q* dynamics [36]. Because Γ_{ph} is directly related to the lattice temperature [9], the hot phonon effects can be excluded.

The above analyses lead us to conclude that the temporally-delayed TSS electron is the key contributor to the observed 1/*q* dynamics. Numerous prior investigations have indeed shown that the electron density in the TSS rises via transition from the bulk to the TSS [16,21,29–34]. In our case, the time scale of this transition is about 1 ps (see again the upper and middle panels of Fig. 3(b)). As illustrated in Fig. 3(c), 1/*q* increases substantially only when $\Delta t > 1$ ps after a large amount of electrons is scattered from the bulk to the TSS; the increased electron density in the TSS at $\Delta t < 1$ ps is too small to cause a significant change in 1/*q*. Note that this 1 ps time scale is much faster than that of the nominal Bi_2Se_3 dynamics (~ 4 ps) [21]. Of course, this is because the spatial overlap between the bulk and the surface of the In = 4%

sample is much larger than that of the nominal Bi_2Se_3 TIs. It also should be mentioned that the measured D_{Drude} dynamics do not directly reflect the electronic transition from the bulk to the TSS, because the THz response collectively measures the photoexcited electron density both in the bulk and in the TSS [21]. Furthermore, the pump-intensity-dependent measurements (Fig. 3(d) and 3(e)) reveal that the maximum $1/q$ increases with increasing the pump fluence which also qualitatively agrees with recent experimental [40] and theoretical [41] investigations on the density-dependent electron-phonon coupling in TIs. Here, we can deduce an important implication of our measurements: the asymmetry of Fano resonance should be tunable by controlling the interaction strength of the phonon mode with the TSS electrons—that is, by using the topological phase transition.

To verify the topological origin of the Fano resonance, we have performed In-concentration-dependent optical-pump THz-probe spectroscopy across the topological quantum critical point, by which we control the interaction strength between the TSS electrons and the bulk optical phonon. All samples are measured with the same pump photon energy (1.55 eV) and fluence (150 $\mu J/cm^2$). Figure 4(a) displays the temporally-resolved Re(G) spectra for In = 0 % (left), 4 % (middle), and 10 % (right), respectively. We clearly see that $1/q$ increases considerably, only when the TSS-bulk spatial overlap is large (i.e. In = 4 %). For In = 0 %, although the optical excitation largely changes the Drude background, the phonon resonance keeps almost the symmetric shape, compared to that of In = 4 % sample. This can be attributed to the relatively small TSS-bulk spatial overlap in the In = 0 % sample, which effectively hinders the coupling of TSS electrons with the bulk phonon. For the In = 10 % sample, where no TSS exists, the symmetry of phonon lineshape is almost unchanged upon photoexcitation. Note that whereas the amount of increased Drude weight for In = 10 % is comparable to those of other samples (maximum differential Drude weight ΔD_{Drude} are 640,

580 and $612\times10^3\times\mathrm{THz}^2\times\mathrm{QL}$ for In = 0 %, 4 % and 10 %, respectively), the relatively small change in the background spectrum for In =10 % is due to broad linewidth of the Drude response (see Fig. 2(e)). Thus, the small $1/q$ of the In = 10 % sample originates from the absence of the TSS states, not from the inefficient photodoping effect in the bulk. For the decay dynamics, we see that decay becomes faster with increasing In-concentration, which may be related to doping induced defects or inhomogeneity (see Ref. [19]).

Additional corroboration for the topologically tunable Fano resonance can be obtained by showing Re(G) with maximum $1/q$ as a function of the In-concentration. Figures 4(b) and 4(c) are the normalized Re(G) responses and the corresponding $1/q$, respectively. For each In-concentration, we selected the transient Re(G) spectrum exhibiting the nearly maximum $1/q$ among the measured pump-probe delays. As expected, $1/q$ increases within the topological phase (In < 6 %), and abruptly subsides in the non-topological phase (In ≥ 6 %). The differential change of $1/q$ (with and without the optical pump) also exhibits similar dependence on the In-concentration, as shown in the lower panel of Fig. 4(c). Given the identical photoexcitation condition, the increased asymmetry in the In = 2 % and 4 % samples cannot be attributed solely to the bulk electrons, because almost the same amount of electrons are initially injected into the bulk conduction band for all the samples. The result is in line with a recently reported transport measurement of Bi_2Se_3 thin crystals in ref. [42]; while the TSS-dominated transport exhibits a strong coupling with optical phonon at ~2 THz, such a behavior was not observed when the transport is dominated by the non-topological bulk electrons.

IV. OUTLOOK

Unlike other tunable Fano systems [13,37,38], our experiments reveal that the Fano resonance exhibits a largely different THz response depending on the topological phase transition. The process is closely related to the controlled coupling strength between the continuous TSS electronic transition and the bulk phonon mode. Across the topological quantum critical point, the pronounced changes of a bulk-TSS spatial overlap is the key for determining the degree of Fano asymmetry. Looking to the future, the observed tunable Fano resonances are mainly spanned in the THz frequency range and rapid optical manipulation is possible with a ps time scale. This indicates that controlling the topological phase transition in $(Bi_{1-x}In_x)_2Se_3$ may become a novel material platform to realize optically tunable topological Fano devices.

ACKNOWLEDGMENT

The work at Yonsei was supported by National Research Foundation of Korea (NRF) through the government of Korea (MSIP) (Grants No. NRF-2011-0013255, No. NRF-2011-D00052, NRF-2009-0083512 and WCI 2011-001), Global Frontier Program (2014M3A6B3063709), the Yonsei University Yonsei-SNU Collaborative Research Fund of 2014, and the Yonsei University Future-leading Research Initiative of 2014. M.B., N.K., and S.O. were supported by the National Science Foundation (NSF Grant No. DMR-0845464) and the Office of Naval Research (Grant No. ONR N000141210456). J.H.S., and M.-H.J. were supported by Institute for Basic Science (IBS), Korea under the contract number of IBS-R014-G1.

APPENDIX A: SAMPLE PREPARATION

High quality epitaxial thin films of $(Bi_{1-x}In_x)_2Se_3$ were grown on 1cm × 1cm Al_2O_3 (0001) substrates by molecular beam epitaxy (MBE) using SVTA designed MBE chamber, whose

base pressure was below 2 × 10-10 Torr. Bi, In and Se sources from Alfa Aesar with purity greater than 99.999% were used as source materials. Following the two step growth method developed at Rutgers University [43,44], an initial deposition of 3 QL was done at 135 °C followed by annealing to 300 °C at which temperature rest of the film was deposited. All the sample growth was done in Se rich environment with the ratio of combined Bi and In flux to Se flux maintained at ~ 1:10. In situ Reflection high energy electron diffraction (RHEED) was used to monitor the crystal quality during growth. High quality films with no impurity phase were obtained as indicated by RHEED [8,43,44]. In order to achieve required concentration and thickness, Bi and In sources were calibrated using in situ quartz crystal microbalance and ex situ Rutherford backscattering. Together these calibration methods offer accuracy to within 1% of the desired concentration.

APPENDIX B: DRUDE-FANO MODEL

Low-energy free-electron response and asymmetric phonon resonance near 2 THz in $(Bi_{1-x}In_x)_2Se_3$ can be described by the following Drude-Fano model [38],

$$\mathrm{G}(\omega)=\left[-\frac{\omega_{\mathrm{Drude}}^2}{i\omega-\Gamma_{\mathrm{Drude}}}-i\sigma_0\frac{\Gamma_{\mathrm{Fano}}\omega(i-(1/q)^{-1})^2}{\omega^2-\omega_{\mathrm{Fano}}^2+i\Gamma_{\mathrm{Fano}}\omega}-i(\varepsilon_\infty-1)\omega\right]\varepsilon_0 d,$$

where $\omega_{\mathrm{Drude}}(\omega_{\mathrm{Fano}})$ is the plasma (center) frequency of the Drude (Fano) oscillator, $\Gamma_{\mathrm{Drude}}(\Gamma_{\mathrm{Fano}})$ is the scattering rate of the Drude (Fano) model, ε_∞ is the dielectric constant at infinite frequency and d is the sample thickness 50 QL. The second term in bracket denotes the Fano resonance and $1/q$ indicates the spectral asymmetry. The larger absolute value of $1/q$ indicates more asymmetric Fano shape. The spectral weight of Drude response is defined by $\mathrm{D}_{\mathrm{Drude}}=\omega_{\mathrm{Drude}}^2 d/(2\pi)^2$ following Wu *et al.* [9].

APPENDIX C: TIME-RESOLVED FANO INTERFERENCE DYNAMICS IN THE SMALL TSS-BULK OVERLAP REGIME

In the main text, we show that the rising transient of $1/q$ under photoexcitation lags behind that of D_{Drude} in the In = 4 % sample (Fig. 3(b) and 3(c)), and the corresponding 1 ps delay is faster than the typical time scale of electron scattering from bulk to TSS in nominal Bi_2Se_3 (~ 4 ps); it is expected that the larger TSS-bulk spatial overlap via In substitution enables faster photodoping of TSS in the In = 4 % sample. There, the rising transient of $1/q$ should become slower as the TSS-bulk overlap is reduced. To confirm this issue, we compare the time-resolved dynamics of $1/q$ and D_{Drude} for In = 0 % and 2 % samples, where the TSS-bulk overlap of these samples is relatively smaller than that of In = 4 % sample. For the In = 0 % sample, because the magnitude of the photoinduced change in $1/q$ is small (almost comparable to the error bar), it is not possible to exactly resolve the time mismatch relative to the D_{Drude} dynamics (top panel of Fig. 5(a)); although the data indeed show a rather slow rising transient of $1/q$ (bottom panel of Fig. 5(a)). On the other hand, for the In = 2 % sample, the change in $1/q$ is sufficiently large such that we clearly resolve the slow rising. We see that while D_{Drude} reaches its maximum at Δt = 1.5 ps (top panel of Fig. (b)), the peak values of $1/q$ emerges at Δt = 3.5 – 4.5 ps (bottom panel of Fig. 5(b)). This shows that the rise transient of $1/q$ lags behind that of D_{Drude}, and corresponding temporal delay is about 2 – 3 ps. which is longer than that of ~ 1 ps time scale in In = 4 % sample, as expected.

REFERENCES

[1] M. Z. Hasan and C. L. Kane, Rev. Mod. Phys. **82**, 3045 (2010).

[2] X. L. Qi and S. C. Zhang, Phys. Today **63**, 33 (2010).

[3] L. Fu, C. L. Kane, and E. J. Mele, Phys. Rev. Lett. **98**, 106803 (2007).

[4] M. König, S. Wiedmann, C. Brüne, A. Roth, H. Buhmann, L. W. Molenkamp, X.-L. Qi, and S.-C. Zhang, Science **318**, 766 (2007).

[5] S.-Y. Xu, Y. Xia, L. a Wray, S. Jia, F. Meier, J. H. Dil, J. Osterwalder, B. Slomski, A. Bansil, H. Lin, R. J. Cava, and M. Z. Hasan, Science **332**, 560 (2011).

[6] T. Sato, K. Segawa, K. Kosaka, S. Souma, K. Nakayama, K. Eto, T. Minami, Y. Ando, and T. Takahashi, Nat. Phys. **7**, 840 (2011).

[7] S. Souma, M. Komatsu, M. Nomura, T. Sato, A. Takayama, T. Takahashi, K. Eto, K. Segawa, and Y. Ando, Phys. Rev. Lett. **109**, 186804 (2012).

[8] M. Brahlek, N. Bansal, N. Koirala, S.-Y. Xu, M. Neupane, C. Liu, M. Z. Hasan, and S. Oh, Phys. Rev. Lett. **109**, 186403 (2012).

[9] L. Wu, M. Brahlek, R. Valdés Aguilar, a. V. Stier, C. M. Morris, Y. Lubashevsky, L. S. Bilbro, N. Bansal, S. Oh, and N. P. Armitage, Nat. Phys. **9**, 410 (2013).

[10] U. Fano, Phys. Rev. **124**, 1866 (1961).

[11] B. Luk'yanchuk, N. I. Zheludev, S. a Maier, N. J. Halas, P. Nordlander, H. Giessen, and C. T. Chong, Nat. Mater. **9**, 707 (2010).

[12] M. Kroner, a O. Govorov, S. Remi, B. Biedermann, S. Seidl, A. Badolato, P. M. Petroff, W. Zhang, R. Barbour, B. D. Gerardot, R. J. Warburton, and K. Karrai, Nature **451**, 311 (2008).

[13] T.-T. Tang, Y. Zhang, C.-H. Park, B. Geng, C. Girit, Z. Hao, M. C. Martin, A. Zettl, M. F. Crommie, S. G. Louie, Y. R. Shen, and F. Wang, Nat. Nanotechnol. **5**, 32 (2010).

[14] P. Fan, Z. Yu, S. Fan, and M. L. Brongersma, Nat. Mater. **13**, 471 (2014).

[15] P. Di Pietro, M. Ortolani, O. Limaj, A. Di Gaspare, V. Giliberti, F. Giorgianni, M. Brahlek, N. Bansal, N. Koirala, S. Oh, P. Calvani, and S. Lupi, Nat. Nanotechnol. **8**, 556 (2013).

[16] N. Kumar, B. A. Ruzicka, P. Syers, K. Kirshenbaum, J. Paglione, and H. Zhao, Phys. Rev. B **83**, 235306 (2011).

[17] J. Linder, T. Yokoyama, and A. Sudbø, Phys. Rev. B **80**, 205401 (2009).

[18] L. Ren, Q. Zhang, J. Yao, Z. Sun, R. Kaneko, Z. Yan, S. Nanot, Z. Jin, I. Kawayama, M. Tonouchi, J. M. Tour, and J. Kono, Nano Lett. **12**, 3711 (2012).

[19] See Supplemental Material, which includes Refs. [45-50].

[20] R. V Aguilar, A. V Stier, W. Liu, L. S. Bilbro, D. K. George, N. Bansal, L. Wu, J. Cerne, A. G. Markelz, S. Oh, and N. P. Armitage, Phys. Rev. Lett. **108**, 87403 (2012).

[21] S. Sim, M. Brahlek, N. Koirala, S. Cha, S. Oh, and H. Choi, Phys. Rev. B **89**, 165137 (2014).

[22] J. A. Sobota, S.-L. Yang, D. Leuenberger, a. F. Kemper, J. G. Analytis, I. R. Fisher, P. S. Kirchmann, T. P. Devereaux, and Z.-X. Shen, Phys. Rev. Lett. **113**, 157401 (2014).

[23] P. Di Pietro, F. M. Vitucci, D. Nicoletti, L. Baldassarre, P. Calvani, R. Cava, Y. S. Hor, U. Schade, and S. Lupi, Phys. Rev. B **86**, 045439 (2012).

[24] A. D. LaForge, A. Frenzel, B. C. Pursley, T. Lin, X. F. Liu, J. Shi, and D. N. Basov, Phys. Rev. B **81**, (2010).

[25] S. V Dordevic, M. S. Wolf, N. Stojilovic, H. Lei, and C. Petrovic, **075501**, (2013).

[26] M. Bianchi, D. Guan, S. Bao, J. Mi, B. B. Iversen, P. D. C. King, and P. Hofmann, Nat. Commun. **1**, 128 (2010).

[27] B. C. Chapler, K. W. Post, A. R. Richardella, J. S. Lee, J. Tao, N. Samarth, and D. N. Basov, Phys. Rev. B **89**, 235308 (2014).

[28] Recently, we become aware of a time-resolved ARPES experiment of Bi_2Se_3; a red-shifted surface A_{1g} phonon mode was reported. In our study, however, no such an additional phonon mode was observed [22]. It might be related to relatively weak pump fluence of our measurement ($\leq$180 $\mu J/cm^2$), compared to intense optical excitation ~1600 $\mu J/cm^2$ in ref. [22].

[29] Y. H. Wang, D. Hsieh, E. J. Sie, H. Steinberg, D. R. Gardner, Y. S. Lee, P. Jarillo-Herrero, and N. Gedik, Phys. Rev. Lett. **109**, (2012).

[30] J. a. Sobota, S. Yang, J. G. Analytis, Y. L. Chen, I. R. Fisher, P. S. Kirchmann, and Z.-X. Shen, Phys. Rev. Lett. **108**, 117403 (2012).

[31] M. Hajlaoui, E. Papalazarou, J. Mauchain, G. Lantz, N. Moisan, D. Boschetto, Z. Jiang, I. Miotkowski, Y. P. Chen, A. Taleb-Ibrahimi, L. Perfetti, and M. Marsi, Nano Lett. **12**, 3532 (2012).

[32] C. W. Luo, H. J. Wang, S. A. Ku, H.-J. Chen, T. T. Yeh, J.-Y. Lin, K. H. Wu, J. Y. Juang, B. L. Young, T. Kobayashi, C.-M. Cheng, C.-H. Chen, K.-D. Tsuei, R. Sankar, F. C. Chou, K. A. Kokh, O. E. Tereshchenko, E. V Chulkov, Y. M. Andreev, and G. D. Gu, Nano Lett. **13**, 5797 (2013).

[33] Y. D. Glinka, S. Babakiray, T. a. Johnson, A. D. Bristow, M. B. Holcomb, and D. Lederman, Appl. Phys. Lett. **103**, 151903 (2013).

[34] J. Qi, X. Chen, W. Yu, P. Cadden-Zimansky, D. Smirnov, N. H. Tolk, I. Miotkowski, H. Cao, Y. P. Chen, Y. Wu, S. Qiao, and Z. Jiang, Appl. Phys. Lett. **97**, 182102 (2010).

[35] J. Lee, J. Inoue, and M. Hase, Phys. Rev. Lett. **97**, 157405 (2006).

[36] S. Hunsche, K. Wienecke, T. Dekorsy, and H. Kurz, Phys. Rev. Lett. **75**, 1815 (1995).

[37] O. V Misochko, K. Ishioka, M. Hase, and M. Kitajima, J. Phys. Condens. Matter **19**, 156227 (2007).

[38] N. Dean, J. C. Petersen, D. Fausti, R. I. Tobey, S. Kaiser, L. V. Gasparov, H. Berger, and A. Cavalleri, Phys. Rev. Lett. **106**, 016401 (2011).

[39] J.-C. Deinert, D. Wegkamp, M. Meyer, C. Richter, M. Wolf, and J. Stähler, Phys. Rev. Lett. **113**, 057602 (2014).

[40] C. Chen, Z. Xie, Y. Feng, H. Yi, A. Liang, S. He, D. Mou, J. He, Y. Peng, X. Liu, Y. Liu, L. Zhao, G. Liu, X. Dong, J. Zhang, L. Yu, X. Wang, Q. Peng, Z. Wang, S. Zhang, F. Yang, C. Chen, Z. Xu, and X. J. Zhou, Sci. Rep. **3**, 2411 (2013).

[41] S. Das Sarma and Q. Li, Phys. Rev. B **88**, 081404 (2013).

[42] M. V. B. Costache, I. Neumann, J. F. Sierra, V. Marinova, M. M. Gospodinov, S. Roche, and S. O. Valenzuela, Phys. Rev. Lett. **112**, 086601 (2014).

[43] N. Bansal, Y. S. Kim, E. Edrey, M. Brahlek, Y. Horibe, K. Iidad, M. Tanimura, G. H. Li, T. Feng, H. D. Lee, T. Gustafsson, E. Andrei, and S. Oh, Thin Solid Films **520**, 224 (2011).

[44] N. Bansal, Y. S. Kim, M. Brahlek, E. Edrey, and S. Oh, Phys. Rev. Lett. **109**, 116804 (2012).

[45] P. Di Pietro, F. M. Vitucci, D. Nicoletti, L. Baldassarre, P. Calvani, R. Cava, Y. S. Hor, U. Schade, and S. Lupi, Phys. Rev. B **86**, 045439 (2012).

[46] A. Damascelli, K. Schulte, D. van der Marel, and A. A. Menovsky, Phys. Rev. B **55**, R4863 (1997).

[47] A. Crepaldi, F. Cilento, B. Ressel, C. Cacho, J. C. Johannsen, M. Zacchigna, H. Berger, P. Bugnon, C. Grazioli, I. C. E. Turcu, E. Springate, K. Kern, M. Grioni, and F. Parmigiani, Phys. Rev. B **88**, 121404 (2013).

[48] M. Hajlaoui, E. Papalazarou, J. Mauchain, L. Perfetti, a Taleb-Ibrahimi, F. Navarin, M. Monteverde, P. Auban-Senzier, C. R. Pasquier, N. Moisan, D. Boschetto, M. Neupane, M. Z. Hasan, T. Durakiewicz, Z. Jiang, Y. Xu, I. Miotkowski, Y. P. Chen, S. Jia, H. W. Ji, R. J. Cava, and M. Marsi, Nat. Commun. **5**, 3003 (2014).

[49] J. Liu and D. Vanderbilt, Phys. Rev. B **88**, 224202 (2013).

[50] P. A. George, J. Strait, J. Dawlaty, S. Shivaraman, M. Chandrashekhar, F. Rana, and M. G. Spencer, Nano Lett. **8**, 4248 (2008).

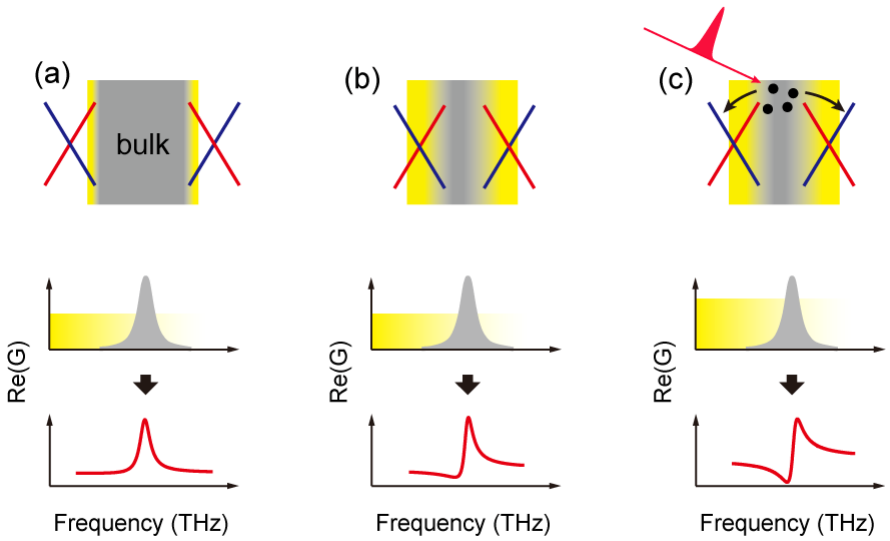

FIG. 1. Schematics for tunable Fano resonance using topological phase transition. (a-c) Upper schematics illustrate side views of TIs. TSSs with Dirac-like energy-momentum dispersions (red and blue lines) and normal bulk insulators (gray squares) coexist. Yellow-shaded regions denote the TSS wavefunctions. Lower schematics display Re(G) spectra in THz range. When the symmetric bulk-phonon resonance (gray region) interacts with the continuum-like Drude transitions of TSSs (yellow regions), the resonance exhibits characteristic Fano asymmetry (red lines). While the interference shape is almost symmetric in a normal TI (a), the Fano asymmetry is stronger as increasing the spatial overlap between the TSS wavefunctions and the bulk (b). When the TSS-bulk spatial overlap is large, the Fano quantum interference can be optically modulated on a ultrafast time scale (c). The photoexcited electrons (black dots) in the bulk are scattered into the TSS state, resulting in the ultrafast dynamic changes of the Fano resonance (see main text).

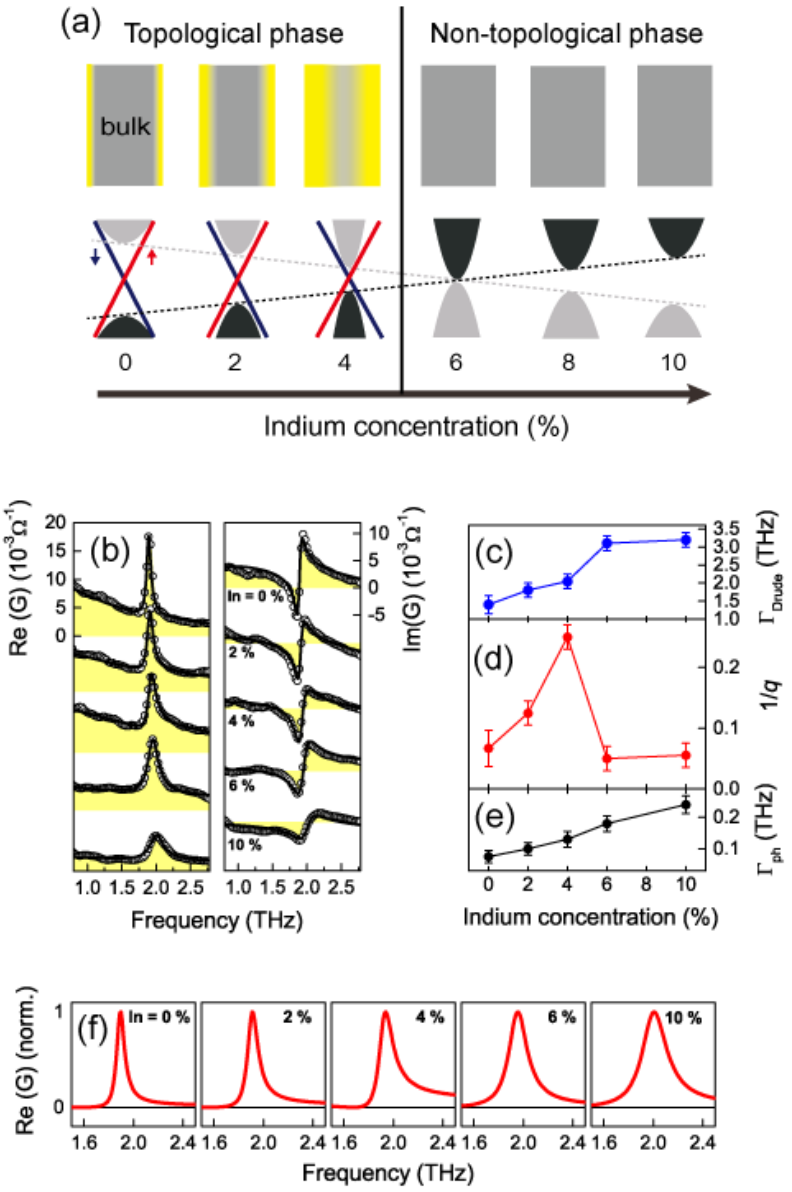

FIG. 2. Equilibrium measurements of Fano resonance in $(Bi_{1-x}In_x)_2Se_3$. (a) Schematics illustrating the In-concentration-dependent topological phase transition, and the associated spatial overlap between the TSS wavefunctions (yellow regions) and the bulk (gray squares). In a topological phase (In = 0, 2, 4 %), linear Dirac dispersion exists as illustrated by blue and red lines. Bulk energy gap between the conduction-band-minimum (gray shaded parabola) and the valence-band-maximum (black shaded parabola) shrinks with increasing the In-

concentration, resulting in the increased overlap between the TSS wavefunctions and the bulk. With more In-concentration (In ≥ 6 %), the transition from the topological phase to the non-topological phase takes place. (b) In-concentration-dependent real (left column, Re(G)) and imaginary (right column, Im(G)) parts of the THz sheet conductance of 50 QL $(Bi_{1-x}In_x)_2Se_3$ measured at 78 K. Black lines are fits obtained by the Drude-Fano model (see main text). (c-e) Drude scattering rate (Γ_{Drude} , blue dots in (c)), Fano asymmetry ($1/q$, red dots in (d)) and phonon linewidth (Γ_{ph} , black dots in (e)) from Drude-Fano fit. (f) In-concentration-dependent normalized Fano fits. The Drude backgrounds are eliminated. The Fano asymmetry strongly is increased as the TSS-bulk spatial overlap increases in the topological phase (In < 6 %). The asymmetry is abruptly vanished as the TSSs disappear in the non-topological phase (In ≥ 6 %).

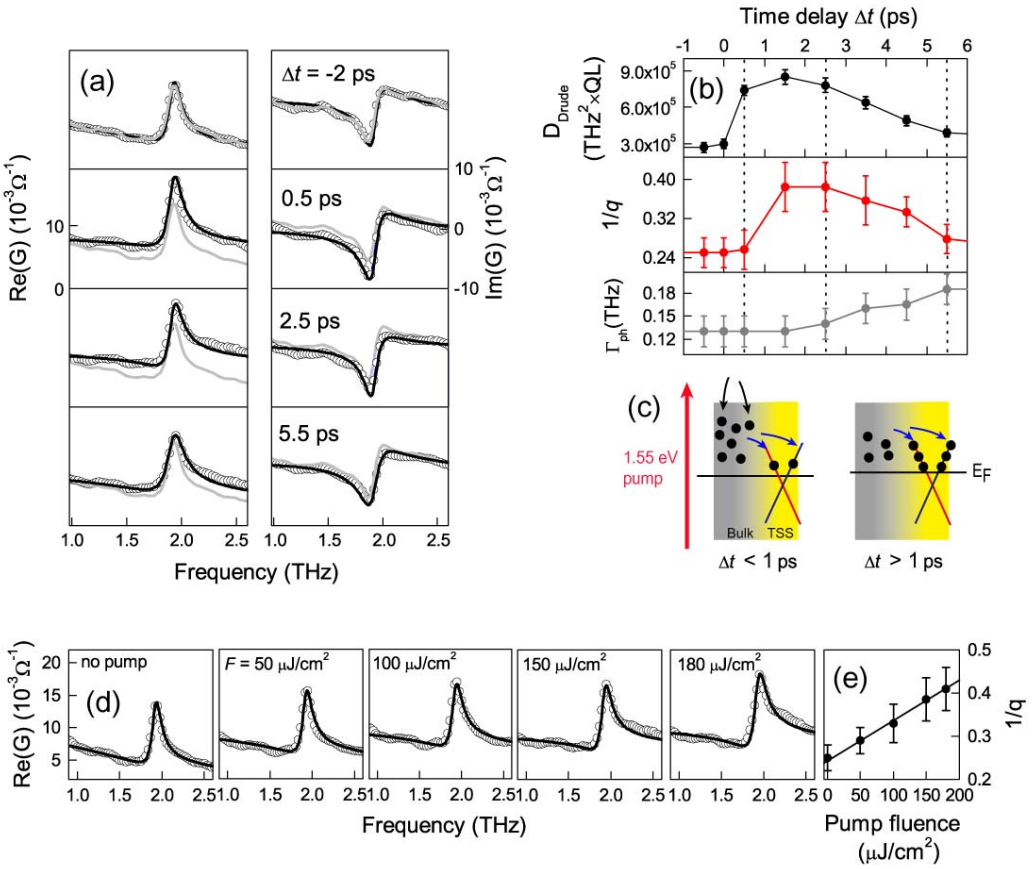

FIG. 3. Time-resolved Fano resonance in $(Bi_{0.96}In_{0.04})_2Se_3$. (a) Real (left column, Re(G)) and imaginary (right column, Im(G)) part of transient THz sheet conductance (black circles) are displayed at different Δt , measured at 78 K with 50 fs, 1.55 eV optical excitation. The black and gray lines are fits obtained from the Drude-Fano model and the equilibrium sheet conductance in Figure 2b, respectively. We clearly see the time evolution of the Fano asymmetry as well as the Drude response. (b) Time-resolved dynamics of Drude weight (D_{Drude}, top panel), Fano asymmetry ($1/q$, middle panel) and phonon linewidth (Γ_{Drude}, bottom panel). The dashed lines indicate the pump-probe time delays Δt at which the time-resolved G spectra are displayed in (a). (c) Schematics illustrating the dynamics of photoexcited electrons (black dots) with 1.55 eV optical excitation (red arrow). The yellow and gray regions denote the TSS wavefunctions and the bulk, respectively. The blue and red lines are

the linear Dirac-like dispersion at the surface. The photoexcited electrons relax to the states near the Fermi level (E_F) in the bulk conduction band (black arrows). Although some of them are scattered to the TSS (blue arrows) before Δt = 1 ps, the electron density at the TSS significantly increases when Δt > 1 ps, which leads to the increased Fano asymmetry. (d,e) Pump-fluence-dependent Re(G) spectra for a fixed time delay at Δt = 2.5 ps (d) and the corresponding $1/q$ (e) are displayed. Black solid line in (e) is a guide to the eye.

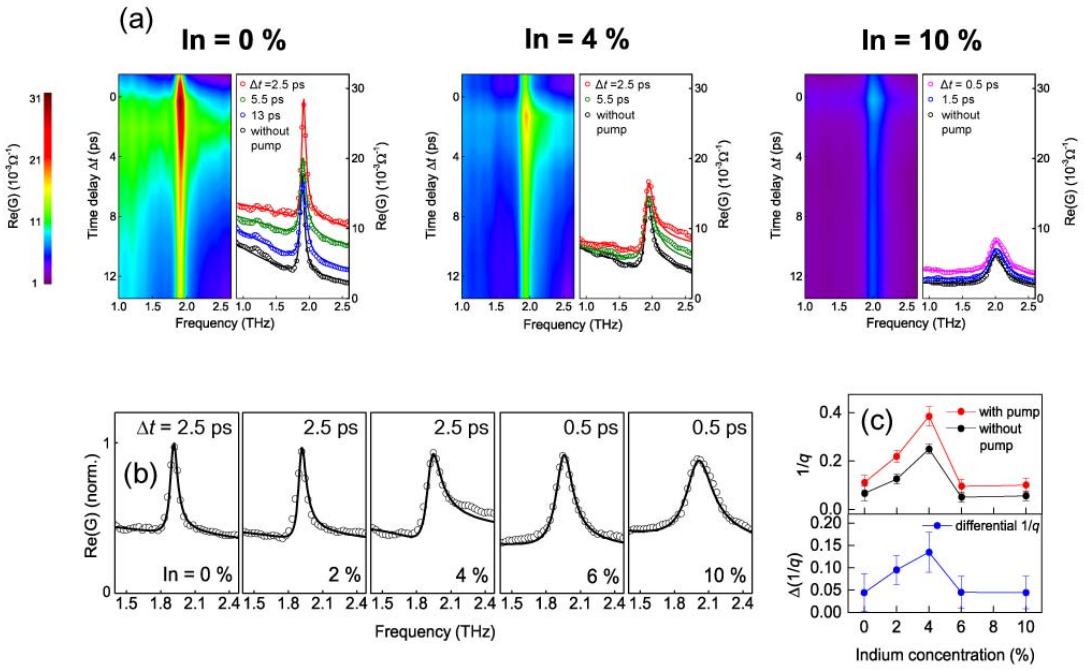

FIG. 4. Topologically tunable, transient Fano resonance using topological phase transition. (a) Contour plots of Re(G) dynamics and line-cut spectra at several Δt for In concentration of 0 % (left), 4 % (middle) and 10 % (right) samples are shown. Note that, while the sample with In = 4 % clearly shows increased Fano asymmetry (middle), the samples with In = 0 % (left) and 10 % (right) do not exhibit such large changes due to the relatively small TSS-bulk spatial overlap and the absence of TSS, respectively. (b) Normalized In-concentration-dependent Re(G) spectra under same optical excitation condition (photon energy = 1.55 eV, pump fluence = 150 $\mu J/cm^2$) are shown. (c) In the upper panel, $1/q$ obtained from the fits to the spectra in (b) are shown (red dots), together with those of non-photoexcited samples (black dots). Corresponding differential changes of $1/q$ are displayed in the lower panel.

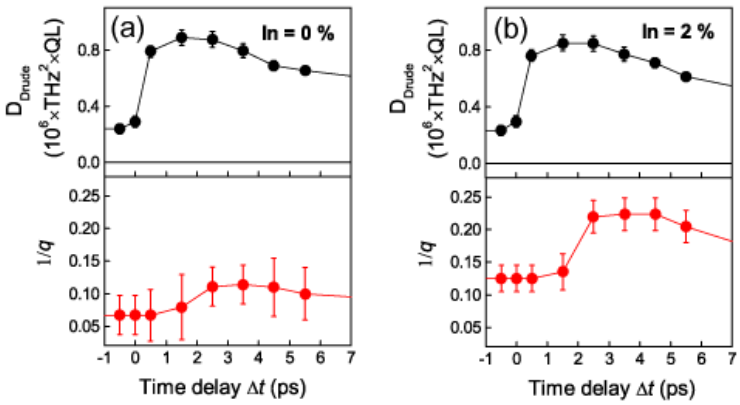

FIG. 5. Time-resolved dynamics of D_{Drude} (black dots in top panels) and $1/q$ (red dots in bottom panels) in In = 0 % (a) and 2 % (b) samples, measured at 78 K with 50 fs, 1.55 eV optical excitation. The pump fluence is 150 μJ/cm^2.